Enteropathogenic *E. coli*-mediated Fast and Coordinated Ca^{2+} responses regulate NF-κB activation

Fangrui Guo[1,2], Roberto Ornelas Guevara[3], Linda Oussaedine[1,2], Geneviève Dupont[3], Laurent Combettes[1,2§], Guy Tran Van Nhieu[1,2§*]

[1]Team "Ca^{2+} signaling and Microbial Infections", Institute for Integrative Biology of the Cell (I2BC), CEA, CNRS UMR9198, Université Paris-Saclay, Gif-sur-Yvette, France

[2]Institut National de la Santé et de la Recherche Médicale U1280, 91190 Gif-sur-Yvette, France.

[3]Unit of Theoretical Chronobiology, Université Libre de Bruxelles, Brussels, Belgium.

[§] Equal contribution

* Corresponding author: guy.tranvannhieu@i2bc.paris-saclay.fr

Running title: EPEC coordinated fast Ca2+ responses

Keywords: EPEC, Calcium, Type III secretion, translocon, ATP

Abstract

Enteropathogenic *Escherichia coli* (EPEC) is a major bacterial enteropathogen causing diarrhea among children in developing countries. Here, we found that EPEC induced isolated Ca^{2+} responses in epithelial cells, triggered by extracellular ATP (eATP). These responses were dependent on type III secretion (T3S) and down-regulated by the bacterial secreted protease EspC, consistent with eATP released by the T3S translocon. By performing high speed Ca^{2+} imaging, we uncovered that at the onset of infection, low eATP levels triggered Ca^{2+}-responses involving the whole cell but showing the small amplitude and fast kinetics usually associated with local Ca^{2+} responses. The findings, supported by theoretical modeling, evocate a conceptual shift whereby low amounts of inositol 1, 4, 5-trisphosphate (IP_3) induced by low eATP levels and subsequent moderate Ca^{2+} release enable the fast coordination of IP_3 receptor cluster activation throughout the cell. Importantly, these yet undescribed coordinated fast responses occurred over prolonged time periods and defined a cell state with dampened activation of the pro-inflammatory transcriptional activator NF-kB associated with a decrease in its Ca^{2+}-dependent O-linked β-N-acetylglucosamine modification.

Introduction

EPEC are diarrheagenic *E. coli* strains that cause significant morbidity and mortality in children under two years of age. While infection rates have significantly declined in industrialized nations, EPEC remains a major public health concern in low-income countries (Lozer et al., 2013). EPEC form attaching and effacing (A/E) lesions on intestinal epithelial cells and lack the ability to produce Shiga toxins or heat-labile (LT) and heat-stable (ST) enterotoxins (Croxen et al., 2013; Gomes et al., 2016; Hazen et al., 2016). The ability of EPEC to form A/E lesions is determined by the locus of Enterocyte Effacement (LEE), a large genomic pathogenicity island that encodes the essential genetic elements required for this process (Pearson et al., 2016). The LEE region of EPEC (E2348/69) encodes components of the type III secretion system (T3SS), a molecular apparatus that translocate at least 25 bacterial effector proteins into the host cell. The EPEC type III secretion system (T3SS) consists of a basal body and a needle-like structure, resembling those found in *Salmonella* and *Shigella*, but with a distinct sheath-like extension at the needle tip, primarily composed of EspA, and about ten times longer than the T3SS needles from other bacterial species. This EspA filament acts as a molecular bridge, extending from the bacterium to the host cell membrane, allowing insertion of the EspB and EspD translocon components into the host cell membrane, enabling type III effectors injection in the cell cytosol (Creasey et al., 2003; Monjarás Feria et al., 2012; Sal-Man et al., 2012). Osmoprotection assays suggest that the translocon forms a pore with an internal diameter ranging between 3 to 5 nm, allowing the passage of unfolded effector proteins into the host cell (Chatterjee et al., 2015). However, the T3SS translocon shows weak pore-forming activity during EPEC infection of epithelial cells, presumably because it forms a sealed conduct between the T3SS and host cell membranes (Guignot et al., 2016). EspC, a secreted serine protease from the autotransporter family, targets EspA and EspD and down-regulates pore formation activity associated with cytotoxicity (Guignot et al., 2015). EPEC T3SS effector proteins translocated into host cells lead are responsible for attaching and effacing (A/E) lesions and intimate bacterial adhesion to the host cells associated with the formation of an actin-rich pedestal formation (Chen & Frankel, 2005).

The detection of pathogenic bacteria by intestinal epithelial cells plays an important role in initiating pro-inflammatory responses. Recognition of bacterial surface components by pattern recognition receptors triggers pro-inflammatory signaling pathways involving the transcriptional activator NF-κB and the production of cytokines such as interleukin-8 and tumor necrosis factor-α (TNF-α) (Edwards et al., 2011). However, EPEC suppresses these signaling pathways early in infection through the coordinated action of several T3SS effector proteins. Among the first translocated T3SS effectors, Tir interacts with TNF-α receptor-associated factors (TRAF2 and TRAF6), recruiting the tyrosine

phosphatases SHP-1 and SHP-2 (Mills et al., 2008; Ruchaud-Sparagano et al., 2011; Yan et al., 2013). Several non-LEE T3SS effectors, including NleE, NleB, NleH1, NleH2, NleC, and NleD, further contribute to inhibiting NF-κB and MAPK signaling. NleE and NleB stabilize the interaction between NFκB and its inhibitory subunit IκB, preventing its degradation, thereby keeping NFκB in an inactive state. The ability of NleE to inhibit NFκB signaling depends on its S-adenosyl-L-methionine (SAM)-dependent methyltransferase activity (Zhang et al., 2011). NleE-mediated methylation of TAB2/3 prevents IKK activation (Zhang et al., 2011). NleB selectively blocks NFκB activation through GlcNAcylation of the TNF-α receptor (TNFR) adaptor protein and TNFR1-associated death domain (TRADD) (S. Li et al., 2013; Pearson et al., 2013). The T3SS effectors NleH1, NleH2 and NleC also interfere with NFκB nuclear translocation (Gao et al., 2009). NleC specifically cleaves P65 RelA (Giogha et al., 2015; Ruchaud-Sparagano et al., 2011; Yen et al., 2010). Interestingly, NleF has been implicated in the activation of NF-κB, underscoring the complexity of the regulation of inflammation during bacterial infection and suggesting the timing of various T3SS effectors' activity (Pallett et al., 2014).

A similar complexity applies to T3SS effectors regulating cell death and survival pathways during EPEC infection of epithelial cells. Tir was found to elicit a rapid Ca^{2+} influx across the host cell membrane, through the activation of a host plasma membrane Ca^{2+} channel, the mechanosensitive transient receptor potential vanilloid 2 (TRPV2) leading to pyroptosis (Zhong et al., 2022). However, the NleA effector, blocks the delivery of TRPV2 channels to the cell surface, thereby dampening Tir-induced Ca^{2+} influx. The effector NleF also directly binds caspase-4 to inhibit its activity (Zhong et al., 2020). The extrinsic apoptotic pathway is triggered by EPEC pili (Abul-Milh et al., 2001). However, the NleD and NleB effectors inhibit this pathway by cleaving JNK and GlcNAcylating the death domain adaptor proteins TRADD and FADD, respectively (Baruch, Gur-Arie, et al., 2011; Pearson et al., 2013). While EspC prevents cytotoxicity linked to pore-formation by the T3SS translocon during the early EPEC infection phases, it was shown to promote intrinsic apoptosis through increase in intracellular Ca^{2+} and calpain activation (Serapio-Palacios & Navarro-Garcia, 2016).

Central to inflammation and cell death / survival pathways induced by EPEC, bacterial-induced Ca^{2+} signals have been a matter of debate. EPEC infection is known to perturb host Ca^{2+} signaling, but the source and sequence of Ca^{2+} signals during infection remain controversial. EPEC was shown to induce Ca^{2+} influx associated with a loss of mitochondrial membranes permeability leading to cell death (Zhong et al., 2020; Ramachandran et al., 2020; Zhong et al., 2022), but was also reported to trigger IP_3-mediated Ca^{2+} release possibly involved in bacterial-induced cytoskeletal rearrangements (Baldwin et al., 1991; Baldwin et al., 1993; Foubister et al., 1994; Bain et al., 1998).

Here, we investigated the characteristics and implications of EPEC-induced Ca^{2+} responses in epithelial cells. We characterized yet undescribed Ca^{2+} signals induced by EPEC and low ATP levels, presenting the fast dynamics and small amplitude of local Ca^{2+} responses but involving large cell area. We found that these responses likely result from the coordination of elementary responses via rapid Ca^{2+}-induced Ca^{2+} release over large cell area, challenging generally admitted concepts on Ca^{2+} diffusion. Importantly, we show that these newly described responses have functional implications by dampening the cell ability to respond to inflammatory signals.

Results

EPEC induces Ca^{2+} responses that depend on Type III secretion-mediated eATP release

Despite their critical role in cellular processes key to bacterial infection, EPEC-induced Ca^{2+} responses remain to be characterized. We therefore set up to perform a detailed single cell imaging of Ca^{2+} responses elicited by cells infected by EPEC.

As shown in Fig. 1, EPEC induced Ca^{2+} transients often corresponding to a single peak of varying amplitude detected over several minutes, with a median corresponding to 6.2 ± 0.8% of the maximal histamine response (Figs. 1A, B). These Ca^{2+} responses were dependent on a functional T3SS, since they were not observed for the T3SS-deficient *escN* mutant (Figs. 1A, C). Only 40 ± 4.7 % of cells, however, elicited responses when challenged wild-type EPEC at a low multiplicity of infection (MOI) of 20 bacteria per cell, a value that raised to 76 ± 4.8 % when using a high MOI of 80 bacteria per cell (Fig. 1C). In contrast, even at the low MOI, more than 83 % of cells showed actin pedestals, indicating that Ca^{2+} responses were elicited only in a fraction of cells targeted by EPEC-type T3SS (Figs. 1D, E). The frequency of Ca^{2+} responses per cell increased over the incubation time with an average frequency of responses per cell raising by 6.9 to 8.3-fold from the first to the last 30 min of EPEC challenge (Fig. 1F). This increased frequency suggested the accumulation of an agonist in the extracellular medium during the course of the infection triggering IP_3-mediated Ca^{2+} release. When pooling all single cell responses, we could observe a steady increase in the average cytosolic Ca^{2+} concentration of the cell population, as previously reported (Ramachandran et al., 2020; Figs. S1B). However, when performing single cell imaging, we did not observe an increase in cytosolic Ca^{2+} basal levels even at high MOI after 2 hours incubation with wild-type bacteria (Fig. S1A).

Together, these results suggest that EPEC induces isolated Ca^{2+} responses that depend on the T3SS for the release of limiting amounts of a Ca^{2+} agonist.

EPEC-mediated Ca^{2+} responses depend on ATP released in the extracellular medium via the T3SS translocon

In previous works, we showed that the EPEC T3SS translocon forms pores in host cell plasma membranes that were down-regulated by the bacterial secreted serine protease EspC (Guignot et al., 2016). We posit that low amounts of ATP released in the extracellular medium by the T3SS translocon were responsible for the isolated Ca^{2+} responses of reduced amplitude elicited by EPEC. According to this view, by removing T3SS translocons from host cell membranes, EspC would down-regulate EPEC-

mediated Ca^{2+} signaling explaining the low ratio of Ca^{2+} responding cells relative to cells forming actin pedestals.

Consistent with this and as shown in Figs. 2A-C, an *espC* mutant induced more Ca^{2+} responses than wild-type EPEC, with 94 ± 3% responding cells and a frequency of 10.5 ± 1.2 responses per cell over the 60 min analysis, compared 40 ± 4.7% responding cells and less than 2 responses per cell for the *espC* mutant and wild-type EPEC, respectively. Also, the average amplitude of Ca^{2+} responses induced by the *espC* mutant was higher than that of wild-type EPEC, suggesting more eATP release (Fig. 1B). Accordingly, cell treatment with Suramin, an inhibitor of purinergic receptors, abolished Ca^{2+} responses induced by the wild-type and *espC* mutant strains (Figs. 2B, C). As expected for ATP-mediated Ca^{2+} release, sample treatment with EGTA, a cell impermeant chelator of extracellular Ca^{2+} did not decrease the percent of Ca^{2+} responding cells triggered by wild-type EPEC or the *espC* mutant (Fig. S2A). The frequency of responses per cell was also not inhibited and even appear to increase upon EGTA-treatment in cells challenged with wild-type EPEC and the *espC* mutant (Figs. S2B, C). In control experiments, Suramin treatment did not affect actin pedestal structures induced by these strains (Fig. S3).

Together, these results suggest that Ca^{2+} responses induced by EPEC are mediated by ATP released in the extracellular medium via pores formed by the T3SS translocon and are down-regulated by EspC.

EPEC induces coordinated Ca^{2+} responses from single IP_3R clusters

We previously showed that *Shigella* induced local Ca^{2+} responses dependent on the T3SS and Ca^{2+} release (Tran Van Nhieu et al., 2013), suggesting that insertion of the Type III translocon was responsible bacterial-induced local Ca^{2+} signals. We therefore set up to investigate whether EPEC could also trigger T3SS-dependent local Ca^{2+} responses.

To explore this, we performed rapid Ca^{2+} imaging at a frequency of 57 ms acquisition per frame to sample elementary Ca^{2+} release events. As shown in Fig. 3, by performing high speed Ca^{2+} imaging, we detected fast Ca^{2+} increases associated with cell challenge with EPEC. These fast Ca^{2+} responses did not correspond to other responses previously reported since they involved the whole cell or a large cell area but show a small amplitude and fast dynamics usually associated with local Ca^{2+} responses (Fig. 3B). As observed for the ATP-dependent responses shown in Fig. 2, the *espC* mutant triggered a higher percent of Ca^{2+} responding cells than wild-type EPEC (Fig. 3C). Also, the response amplitude was higher for the *espC* mutant with an average amplitude corresponding to 7.7 ± 0.4 % (mean ± SEM) of the maximal agonist response, compared to 5.4 ± 0.4 % (mean ± SEM) for wild-type EPEC (Fig. 3E). These responses occurred repeatedly at a high frequency of up to 4.5 responses per minute during

several minutes following bacterial challenge (Figs. 3D and 3F) and were dependent on Type III Secretion, as evidenced by the lack of response in cells infected with the *ΔescN* strain (Figs. 3B and 3C). EPEC-induced fast Ca^{2+} responses were dependent on Ca^{2+} release since they were inhibited by U73122, a PLC inhibitor (Figs. 3C and 3D). These similarities with the EPEC-induced eATP-dependent Ca^{2+} responses suggested that the atypical fast responses were triggered by low amounts of ATP released in the extracellular medium following insertion in host cell plasma membranes of discrete numbers of EPEC T3SS translocons. Consistently, these atypical EPEC-induced fast responses were abolished in the presence of the ATP receptor inhibitor Suramin (Figs. 3C, D).

Together, these results show that at the onset of infection, EPEC induces an atypical pattern of fast Ca^{2+} responses involving the whole or large area of the cell, likely resulting from low ATP levels released by the insertion of a discrete number of translocons in host cell membranes.

EPEC-induced fast Ca^{2+} responses are triggered by low ATP levels

Previous studies have described local Ca^{2+} increases triggered by sub-maximal agonist concentrations and leading to limited IP_3-mediated Ca^{2+} release. These local Ca^{2+} responses are typically small, of short durations and localized to subcellular regions. Among these, the so-called "Blips" correspond to elementary events of opening of a single IP_3 receptor channel usually lasting between 50 and 100 ms, whereas "Puffs" involve the synchronized activation of multiple IP_3 receptor channels in localized clusters and last several hundreds of ms (Swillens et al., 1999). In contrast to these described local Ca^{2+} signals, EPEC-induced fast and small responses could occur throughout the cell, suggesting the coordination of elementary responses over large cell area. Since our findings suggested that these responses were elicited by minute amounts of eATP released by a discrete number of T3SS translocons, we investigated whether low ATP levels could elicit similar responses.

HeLa cells treated with 150 nM ATP showed Ca^{2+} responses that were indistinguishable from fast responses elicited by EPEC, with an average percent of Ca^{2+} responding cells of 61.2 ± 5.8 (median ± SEM) and a frequency of 3.9 responses per cell over 60 seconds (Figs. 4A, C and S4A, B). These fast Ca^{2+} responses had an amplitude that did not exceed 10 % of the maximal agonist response, and occurred over several minutes (Fig. 4A). As observed for EPEC, fast Ca^{2+} responses induced by low ATP levels involved the whole cell or large cell area encompassing the nuclear and perinuclear area and corresponding to at least 30 % of the cell area as illustrated in Fig. 4B. In this large area, all ROIs corresponding to 1 square micron showed a superimposable profile, as illustrated by traces in Fig. 4C. More detailed scrutinizing showed that in their initial mounting phase, these fast Ca^{2+} responses were created by the opening of discrete clusters involving an area of ca. 0.04 μm^2 that had a transient

activity, or possibly were highly mobile, since they were seldom detected at a similar location for three consecutive 22 ms acquisition frames (Fig. S5). These discrete clusters showed similar Ca^{2+} kinetics suggesting the coordination of Ca^{2+} release of single IP_3R clusters throughout the area that we will hereafter termed CCRICs for "Coordinated Ca^{2+} Responses from IP_3R Clusters". Treatment with BAPTA-AM to chelate intracellular Ca^{2+} led to a complete inhibition of CCRICs (N = 3, n > 150 cells; Fig. S4A). Ca^{2+} responses could still be detected upon cell treatment with EGTA-AM consistent with its lower k_{on} rate for Ca^{2+}, but with a significant inhibition of the percentage of Ca^{2+} responding cells as well as of the frequency of responses per cell, suggesting that coordination could occur via Ca^{2+} diffusion and Ca^{2+}-induced Ca^{2+} release (Fig. S4A-C). Local responses elicited by these ATP concentrations could also be detected often occurring at the cell periphery (Figs. 4B, red region and 4C, red arrow). While the CCRICs area and the peripheral puff area showed spatially segregated Ca^{2+} responses at the onset of the elicitation (Fig. 4C, peaks 1, 3 and 2, 4), this spatial segregation appeared to blur over the duration of the experiment with peaks integrating responses from the whole cell (Fig. 4C, green and red dashed lanes).

CCRICs are coordinated by the rapid diffusion of Ca^{2+} at low concentrations in cell area with a high density of IP_3 clusters

In Fig. 5, we used modeling to further investigate the mechanism of coordination of these fast Ca^{2+} responses. Based on our previous studies (Voorsluijs et al., 2019; Ornelas-Guevara et al., 2023), the model provides a fully stochastic spatial description of Ca^{2+} release dynamics from IP_3R clusters in a two-dimensional representation of a HeLa cell. The simulation domain extends on $10 \times 10\ \mu m^2$ and is discretized into a 20×20 grid of compartments ($0.5 \times 0.5\ \mu m^2$ each), each representing a cytosolic subvolume of 10^{-16} L. Each compartment contains at most one cluster of IP_3R, whose dynamics is described as a whole. Besides, cytosolic Ca^{2+} concentration can also vary because of uptake by SERCA, release by a leak or diffusion. A full description of the model can be found in the Supplementary Methods.

In Fig. 5A, low ATP levels lead to low IP_3 levels activating a limited number of IP_3 clusters, opening stochastically and releasing small amounts of Ca^{2+}. In a given area of the cell, the Ca^{2+} variation integrates Ca^{2+} release from clusters within this area, as well as Ca^{2+} diffusing from or to other cell area. For a given response, the initially firing cluster is contained in an area characterized by the highest Ca^{2+} peak amplitude (Fig. 5A, blue and green arrows) that dampens in a distal area (Fig. 5A, blue and green arrowheads). If the density of IP_3R clusters is low, as expected for ER compartment at the cell periphery, the spatial segregation of the initial firing cluster and resulting Ca^{2+} diffusion to other area is clearly detected (Fig. 5A). In instances, however, the model predicts temporally coordinated

responses of similar amplitude, suggesting Ca^{2+}-induced Ca^{2+} release from secondary clusters (Fig. 5A, black arrow). For both type of Ca^{2+} dynamics, a large value of the Ca^{2+} diffusion coefficient of 100 μm^2 / s is a key parameter that needs to be taken into account in the model. While it is generally admitted that Ca^{2+} diffuses very slowly due to the Ca^{2+} buffers in the cell (~30 μm^2/s), the low levels of Ca^{2+} released by CCRICs may not be subjected to the diffusion limitations observed at higher Ca^{2+} levels, because of the relative moderate affinity of buffers for Ca^{2+}.

If the IP_3R cluster density is high, as expected in the large perinuclear and nuclear area corresponding to the bulk of the ER, the coordination between individual clusters is very fast (Fig. 5B). As a result, the identification of initial firing clusters goes beyond the technical capacities of the imaging set-up, and ROI within this area show comparable profiles of fast Ca^{2+} responses (Fig. 5B). Upon prolonged incubation with increasing Ca^{2+} responses and sensitization of IP_3R clusters, the coordination of responses linked to Ca^{2+}-induced Ca^{2+} release becomes predominant throughout the cell (Fig. 5C).

These findings indicate that the novel Ca^{2+} response pattern is not exclusive to EPEC infection and can be replicated by low levels of eATP, suggesting a broader physiological relevance. From an immunological perspective, CCRICs may therefore play a critical role in various signaling pathways during bacterial infection.

Low eATP levels dampen NF-κB activation.

eATP is a well-characterized danger signal contributing to the elicitation of pro-inflammatory signals in various tissues in response to infections (Savio et al., 2018). Previous studies linked intracellular Ca^{2+} signaling and NF-κB activation, a key transcription factor that triggers inflammatory responses (Smedler et al., 2014). We therefore set up to investigate the effects of CCRICs triggered by low eATP levels on NF-κB activation, by performing Western blot analysis against the phosphorylated forms of IκBα (p- IκBα) and P65 (p-P65).

As shown in Figs. 6A and 6B, in control samples, TNF-α induced IκB-α phosphorylation peaking 10 minutes following challenge. In contrast, in the presence of low ATP levels, IκB-α showed a delayed phosphorylation with a 2.1 fold decrease at 10 minutes post-challenge (Figs. 6A and 6B). Consistently, the rates of IκB-α degradation were also slower in the presence of ATP relative to control (Figs. 6A and 6C). As expected from the IκB-α results, TNF-α induced the phosphorylation of the NF-κB P65 subunit and ATP led to a delay and decrease in P65 phosphorylation (Figs. 6D and 6E).

In control experiments, we did not detect differences in P65 phosphorylation in response to TNF-α stimulation when cells were treated with BAPTA-AM to chelate intracellular Ca^{2+} (Figs. 6F and 6H).

However, cell treatment with BAPTA-AM prevented the dampening of P65 phosphorylation triggered by low ATP levels (Figs. 6G and 6H), suggesting that CCRICs down-regulated TNF-α -induced NF-κB activation.

Low eATP levels down-regulates NF-κB activation through Ca^{2+}-dependent O-GlcAcylation

We next investigated how CCRICs could regulate NF-κB activation. O-linked β-N-acetylglucosamine (O-GlcNAc) transferase (OGT) was reported to regulate NF-κB signaling by post-translationally modifying the p65 subunit (Ruan et al., 2017). Interestingly, OGT is regulated by Ca^{2+} signaling, suggesting that CCRICs could affect NF-κB activation via O-GlcNAcylation.

As shown in Fig. S6, TNF-α in the presence of 150 nM eATP stimulated the levels of O-GlcNacylation, specifically for proteins with an apparent molecular weight superior to 100 kDa, that was not observed with TNF-α alone. To further investigate the effects of low eATP levels on NF-κB O-GlcNacylation, we performed immunoprecipitation of P65 RelA on lysates of cells stimulated for 12 minutes with TNF-α alone or co-stimulated with TNF-α and 150 nM eATP. As shown in Fig. 7, TNF-α induced increased O-GlcNacylation of P65 relative to non-stimulated cells, but this increase was inhibited by low eATP levels. Inhibition of P65 O-GlcNacylation by eATP was Ca^{2+} dependent, since it was not observed in the presence of BAPTA-AM (Fig. 7).

The results indicate that low eATP levels inhibit O-GlcNacylation of P65 induced by TNF-α in a Ca^{2+}-dependent manner and suggest that differential O-GlcNacylation of P65 relative to higher molecular weight proteins.

Discussion

We report here the characterization of CCRICs, corresponding to yet undescribed Ca^{2+} responses showing the rapid kinetics and small amplitude of local Ca^{2+} responses but coordinated over large cell area. We found that CCRICs implicate the rapid coordination of IP_3R clusters in large cell area, challenging established concepts in the Ca^{2+} signaling field.

Ca^{2+} diffusion in the cytosol is regulated by mobile and immobile Ca^{2+}-binding proteins acting as buffers and forming localized microdomains with steep Ca^{2+} concentration gradients. At the mouth of an open IP_3R channel, Ca^{2+} concentration can reach 100 µM, while just 1–2 µm away, it may drop below 1 µM. Diffusion is restricted by Ca^{2+} buffers with K_D's that are generally lower than this concentration. Consequently, Ca^{2+} signaling is generally admitted to be spatially restricted, typically influencing regions within approximately 5 µm of the release site (Foskett et al., 2007). The distribution of Ca^{2+}-

binding proteins and the spatial arrangement of release channels allow IP_3R-mediated $[Ca^{2+}]_i$ signals to exhibit diverse spatial and temporal properties, making this system highly adaptable (Vandeput et al., 2007). High-resolution optical imaging of fluorescent Ca^{2+} indicators in intact cells indicates that IP_3-mediated $[Ca^{2+}]_i$ signals are structured levels (Foskett et al., 2007). At low IP_3 levels, individual IP_3R opens stochastically at discrete release sites, causing localized elevations in cytoplasmic $[Ca^{2+}]$. At higher IP_3 levels, Ca^{2+} release spreads between IP_3R clusters, propagating waves that travel at tens of microns per second, coordinating intracellular signaling ultimately leading to a global Ca^{2+} response. In reference models describing intracellular Ca^{2+} dynamics, cell regions with a high IP_3R density initiate the Ca^{2+} response from which Ca^{2+} waves propagate with a diffusion coefficient of 10 – 30 $\mu m^2/s$ (Falcke et al., 2003).

In contrast to these described global and local Ca^{2+} responses, we found CCRICs to be highly temporally coordinated over large area, suggesting the fast diffusion of Ca^{2+} and propagation of Ca^{2+} by Ca^{2+}-induced Ca^{2+} release. While challenging generally admitted concepts on the poor diffusion of Ca^{2+}, this view is fully supported by our theoretical modeling implicating the fast diffusion of Ca^{2+}, with a diffusion coefficient of at least 100 $\mu m^2/s$ that can be expected at low cytoplasmic $[Ca^{2+}]$. Indeed, at these low Ca^{2+} concentrations not exceeding a few hundreds nM, the majority of Ca^{2+} buffers are not expected to efficiently bind to Ca^{2+} and to significantly interfere with Ca^{2+} diffusion because of their relative low affinity.

We found that CCRICs implicate a large cell area including the nuclear and perinuclar area, while local Ca^{2+} responses were detected at small area of the cell periphery. The large CCRIC area likely involves the bulk of the endoplasmic reticulum, while peripheral area may contain smaller ER compartments. In our model considering fast Ca2+ diffusion when buffers are far from saturation, the higher density of IP_3R clusters in the CCRIC area accounts for the high coordination of the responses, relative to the lack of coordination in peripheral area where lower IP_3R density is expected.

We showed that a low dose of eATP triggering CCRICs delayed and dampened NF-κB activation linked to a reduction in O-GlcNAcylation of the NF-κB p65 subunit. One major open question is the mechanism by which CCRICS down-regulate NF-κB activation. NF-κB activity can be modulated by O-GlcNAcylation, a reversible glycosylation modification catalyzed by O-GlcNAc transferase (OGT) and O-GlcNAcase (OGA) (Liu & Ramakrishnan, 2021). Previous studies demonstrated that Ca^{2+} signals activate Ca^{2+}-regulated enzymes like CaMKII, which in turn phosphorylates and activate OGT, promotes O-GlcNAcylation (Ruan et al., 2017). In other studies, OGT-mediated O-GlcNAcylation could modulate NF-κB signaling pathway (X. Dong et al., 2023). O-GlcNAcylation of P65 could also inhibit its interaction with IκB-α, promote p65 nuclear translocation and increase NF-κB transcriptional activity (Liu &

Ramakrishnan, 2021). Reduced O-GlcNAcylation of P65 at residues S550 and S551 was shown to result in decreased NF-κB activation and nuclear translocation (Motolani et al., 2023). These findings are in line with our results suggesting that CCRICs elicited by low-level eATP, downregulate p65 O-GlcNAcylation and NF-κB activation, possibly by modulating OGT activity or OGT-p65 interactions. Reduced O-GlcNAcylation of p65 may affect its phosphorylation patterns indirectly, perhaps by altering the interaction of NF-κB with kinases or phosphatases involved in its activation (Özcan et al., 2010).

Our findings indicate that eATP differentially regulate inflammatory signaling pathways in epithelial cells by dampening NF-κB activation at low levels and stimulating its activation at high concentrations. These results extend the key role of eATP from a danger-associated molecular pattern (DAMP) to a fine-tuner of inflammatory responses depending on its concentration.

Materials and Methods

Cell and Bacterial culture

HeLa cells were maintained in Dulbecco's Modified Eagle Medium (DMEM; Gibco, Thermo Fisher Scientific) supplemented with 10% fetal bovine serum (FBS; Gibco, Thermo Fisher Scientific) at 37 °C in a humidified incubator with 10% CO_2. Wild-type Enteropathogenic Escherichia coli (EPEC WT), *ΔescN*, and *ΔespC* strains were cultured in Luria-Bertani (LB) broth at 37 °C with kanamycin at a final concentration of 15 µg/ml in a shaking incubator. All strains were transformed with the pmCherry-N1 plasmid, which encodes red fluorescent protein and carries an ampicillin resistance gene for selection. Where applicable, ampicillin (100 µg/mL) and kanamycin were included to maintain resistance markers. The red fluorescence enabled visualization of the bacteria during downstream analyses.

EPEC infection of HeLa cells

HeLa cells were seeded in 6-well plates at a density of 4.5×10^5 cells per well one day before infection. EPEC WT, *ΔescN,* and *ΔespC* strains grown in the exponential phase were resuspended and primed for 5 hours before challenging HeLa cells in DMEM medium. Cells were challenged with bacteria at an OD600 = 0.2 (Low MOI) or 0.8 (High MOI).

Ca^{2+} imaging

HeLa cells were seeded onto 25 mm-diameter glass coverslips. Cells were preloaded with the fluorescent indicator dye Cal-520 (AAT #21130) for 30 minutes at room temperature, followed by two PBS washes and one time with DMEM. And placed coverslips, imaging was performed in an observation chamber in DMEM without phenol red, supplemented with 25 mM HEPES. Following a 3-minute

baseline acquisition, add the required bacteria strains and OD600 into the chamber. Following a 10-minute incubation at room temperature to allow bacterial attachment. Imaging was then carried out at 35°C using a Nikon Eclipse TE200 inverted fluorescence microscope with a 60× objective for 1h of infection. Fluorescence signals were acquired 485 nm with excitation and 535 nm emission parameters. Image control and data acquisition were managed by Simple32 software (Compix Inc.), depending on the experiment requirement, imaging at 22ms, 57ms or 10 sec acquisition intervals. 3 µM of Histamine and 2 µM of ionomycin were applied to check the ability of cells to show calcium response. Images were captured using a CMOS camera (Hamamatsu) and analyzed using the same software.

Immunofluorescence analyses

Cells were washed three times with PBS and fixed with 3.7% paraformaldehyde (PFA), permeabilized with 0.1% Triton X-100 for 5 minutes and washed with PBS. Blocking was performed using 3% FBS in PBS for 30 minutes at room temperature. Cells were incubated with primary antibodies for 2 hours: mouse anti-phalloidin (1:200; Fischer Scientific, #17511176). Secondary antibodies (anti-mouse), along with DAPI were applied for 1 hour. Samples were mounted using Dako mounting medium (Agilent) and imaged using a Nikon Ti2 confocal microscope equipped with a 60× objective and Nikon acquisition software.

Modelling

We develop a fully stochastic spatial model to simulate Ca^{2+} release dynamics from IP_3R clusters in a two-dimensional representation of a HeLa cell. The simulation domain measures 10 × 10 μm^2 and is discretized into a 20 × 20 grid of compartments (0.5 × 0.5 μm^2 each), each representing a cytosolic subvolume of 10^{-16} L. Ca^{2+} exchange between the Endoplasmic Reticulum (ER) and the cytosol occurs through IP_3R-mediated release, SERCA uptake, and ER Ca^{2+} leak, following the framework by Voorsluijs et al., 2019 and Ornelas-Guevara et al., 2023. Ca^{2+} diffusion is implemented stochastically as a kinetic process between adjacent compartments (Kraus et al., 1996), with a diffusion coefficient of 100 $\mu m^2/s$ to reflect moderate endogenous buffering. Each IP_3R cluster functions as a single unit with four possible states: Open (O), Closed (C) and two Inhibited states (i1, and i2), transitioning in response to local [Ca^{2+}] and [IP_3]. This phenomenological description captures key characteristics of Ca^{2+} puffs and their transition to global signals via Ca^{2+} diffusion and Calcium Induced Calcium Release.

We perform all simulations using the Gillespie algorithm, where each event, reaction or diffusion, is selected stochastically based on its propensity. See Supplementary Methods for complete model equations and parameter values.

Western Blot analysis

To obtain total cell extracts, cells were lysed in sample buffer 1x (62.5 mM Tris pH=8, 2% SDS, 10% glycerol, 0.05% bromophenol blue, 5% β- mercaptoethanol) and boiled at 95°C for 5 minutes. Proteins from total lysates were separated by SDS PAGE and transferred to nitrocellulose membrane (0.45µM AmershamTM ProtranTM). Western Blot analysis was performed according to standard procedure using the following primary antibodies: IkappaBalpha (OZYME, 9424S), Phospho-IκB-α (OZYME, 9424S), NF-kappaB p65 (OZYME, 9246S), Phospho-NF-kappaB p65 (OZYME, 3033S), HSP90 (Santa Cruz Biotechnologies sc-13119). HRP-conjugated anti-mouse (Cytiva) and anti-rabbit (Sigma) were used as secondary antibodies.

Immunoprecipitation assays

HeLa cells were seeded in 150 cm^2 dishes (7.4×10^6 cells/dish) and cultured in DMEM supplemented with 10% FBS. Cells were pretreated with 20 µM BAPTA for 30 minutes at room temperature where indicated, then stimulated with 10 ng/mL TNF-α alone or in combination with 150 nM ATP for an additional 12 minutes. After treatment, cells were washed with ice-cold PBS containing 1 mM NaF and 1 mM Na_3VO_4, lysed in ice-cold lysis buffer (50 mM Tris-HCl pH 7.5, 0.5% Triton X-100, 100 mM NaCl, 1 mM DTT, protease inhibitor cocktail without EDTA), and incubated on a rotating wheel at 4°C for 1 hour. Lysates were clarified by centrifugation at 13,000 rpm for 30 minutes at 4°C. Supernatants were incubated with 5 µL of anti-NF-kB p65 antibody (Abcam, ab16502) for 2 hours at 4°C with rotation, followed by overnight incubation with pre-equilibrated protein A/G beads. Immunocomplexes were washed once with lysis buffer and twice with PBS, then eluted in Laemmli buffer by boiling at 100°C for 5 minutes. Input and IP samples were analyzed by Western blotting using antibodies against O-GlcNAc (Abcam, ab2739), anti-NF-kB p65 (OZYME, 9246S), and Actin (OZYME, 4967).

Statistical Analysis

All quantitative data are presented as mean ± SEM from at least three independent experiments. Statistical significance was assessed using unpaired two-tailed Student's t-tests with unequal variance, unless otherwise specified. GraphPad Prism 7 (GraphPad Software) was used for statistical analysis, and p-values < 0.05 were considered statistically significant.

Acknowledgments

This work was funded by the Inserm, CNRS and ANR programs CALPLYCX and VITAL to GTVN. FG was funded by a Chinese Science Council PhD fellowship. ROG was supported by Wallonie-Bruxelles International (Excellence Grant 2025). This work was supported by a PDR FRS-FNRS project

(T.0073.21). GD is Research Director at the Belgian "Fonds National pour la Recherche Scientifique" (FRS-FNRS).

Author contribution

FR, LC and GTVN designed, performed experiments and wrote the mansucript. LO performed experiments. ROG and GD performed the mathematical modeling.

Competing Interests

The authors declare no conflict of interest.

References

Abul-Milh, M., Wu, Y., Lau, B., Lingwood, C. A., & Foster, D. B. (2001). Induction of Epithelial Cell Death Including Apoptosis by Enteropathogenic Escherichia coli Expressing Bundle-Forming Pili. *Infection and Immunity*, *69*(12), 7356–7364. https://doi.org/10.1128/IAI.69.12.7356-7364.2001

Bain C, Keller R, Collington GK, Trabulsi LR, Knutton S. Increased levels of intracellular calcium are not required for the formation of attaching and effacing lesions by enteropathogenic and enterohemorrhagic Escherichia coli. Infect Immun. 1998 Aug;66(8):3900-8. doi: 10.1128/IAI.66.8.3900-3908.1998. PMID: 9673278; PMCID: PMC108447.

Baldwin, T. J., Ward, W., Aitken, A., Knutton, S., & Williams, P. H. (1991). Elevation of intracellular free calcium levels in HEp-2 cells infected with enteropathogenic Escherichia coli. *Infection and Immunity*, *59*(5), 1599–1604. https://doi.org/10.1128/iai.59.5.1599-1604.1991

Baldwin TJ, Lee-Delaunay MB, Knutton S, Williams PH. Calcium-calmodulin dependence of actin accretion and lethality in cultured HEp-2 cells infected with enteropathogenic Escherichia coli. Infect Immun. 1993 Feb;61(2):760-3. doi: 10.1128/iai.61.2.760-763.1993. PMID: 8423102; PMCID: PMC302790.

Brown MD, Bry L, Li Z, Sacks DB. Actin pedestal formation by enteropathogenic Escherichia coli is regulated by IQGAP1, calcium, and calmodulin. J Biol Chem. 2008 Dec 12;283(50):35212-22. doi: 10.1074/jbc.M803477200. Epub 2008 Sep 22. PMID: 18809683; PMCID: PMC2596374.

Baruch, K., Gur-Arie, L., Nadler, C., Koby, S., Yerushalmi, G., Ben-Neriah, Y., Yogev, O., Shaulian, E., Guttman, C., Zarivach, R., & Rosenshine, I. (2011). Metalloprotease type III effectors that specifically cleave JNK and NF-κB. *The EMBO Journal*, *30*(1), 221–231. https://doi.org/10.1038/emboj.2010.297

Chatterjee, A., Caballero-Franco, C., Bakker, D., Totten, S., & Jardim, A. (2015). Pore-forming Activity of the Escherichia coli Type III Secretion System Protein EspD. *The Journal of Biological Chemistry*, *290*(42), 25579–25594. https://doi.org/10.1074/jbc.M115.648204

Chen, H. D., & Frankel, G. (2005). Enteropathogenic Escherichia coli: Unravelling pathogenesis. *FEMS Microbiology Reviews*, *29*(1), 83–98. https://doi.org/10.1016/j.femsre.2004.07.002

Clapham, D. E. (2007). Calcium Signaling. *Cell*, *131*(6), 1047–1058. https://doi.org/10.1016/j.cell.2007.11.028

Crane, J. K., Olson, R. A., Jones, H. M., & Duffey, M. E. (2002). Release of ATP during host cell killing by enteropathogenicE. coli and its role as a secretory mediator. *American Journal of Physiology-Gastrointestinal and Liver Physiology*, *283*(1), G74–G86. https://doi.org/10.1152/ajpgi.00484.2001

Creasey, E. A., Delahay, R. M., Daniell, S. J., & Frankel, G. (2003). Yeast two-hybrid system survey of interactions between LEE-encoded proteins of enteropathogenic Escherichia coli. *Microbiology (Reading, England)*, *149*(Pt 8), 2093–2106. https://doi.org/10.1099/mic.0.26355-0

Croxen, M. A., Law, R. J., Scholz, R., Keeney, K. M., Wlodarska, M., & Finlay, B. B. (2013). Recent advances in understanding enteric pathogenic Escherichia coli. *Clinical Microbiology Reviews*, *26*(4), 822–880. https://doi.org/10.1128/CMR.00022-13

Dong, X., Shu, L., Zhang, J., Yang, X., Cheng, X., Zhao, X., Qu, W., Zhu, Q., Shou, Y., Peng, G., Sun, B., Yi, W., Shu, Q., & Li, X. (2023). Ogt-mediated O-GlcNAcylation inhibits astrocytes activation through modulating NF-κB signaling pathway. *Journal of Neuroinflammation*, *20*(1), 146. https://doi.org/10.1186/s12974-023-02824-8

Dupont, G., Combettes, L., Bird, G. S., & Putney, J. W. (2011). Calcium oscillations. *Cold Spring Harbor Perspectives in Biology*, *3*(3), a004226. https://doi.org/10.1101/cshperspect.a004226

Edwards L. A., Bajaj-Elliott M., Klein N. J., Murch S. H., & Phillips A. D. (2011). Bacterial-Epithelial Contact Is a Key Determinant of Host Innate Immune Responses to Enteropathogenic and Enteroaggregative Escherichia coli. *PLOS ONE*, *6*(10), e27030. https://doi.org/10.1371/journal.pone.0027030

Falcke, M. (2003). Deterministic and stochastic models of intracellular Ca^{2+} waves. *New J. Phys.* 5 96. https://doi.org/10.1088/1367-2630/5/1/396

Foskett, J. K., White, C., Cheung, K.-H., & Mak, D.-O. D. (2007). Inositol Trisphosphate Receptor Ca2+ Release Channels. *Physiological Reviews*, *87*(2), 593–658. https://doi.org/10.1152/physrev.00035.2006

Foubister V, Rosenshine I, Finlay BB. A diarrheal pathogen, enteropathogenic Escherichia coli (EPEC), triggers a flux of inositol phosphates in infected epithelial cells. J Exp Med. 1994 Mar 1;179(3):993-8. doi: 10.1084/jem.179.3.993. PMID: 8113690; PMCID: PMC2191415.

Gao, X., Wan, F., Mateo, K., Callegari, E., Wang, D., Deng, W., Puente, J., Li, F., Chaussee, M. S., Finlay, B. B., Lenardo, M. J., & Hardwidge, P. R. (2009). Bacterial Effector Binding to Ribosomal Protein S3 Subverts NF-κB Function. *PLoS Pathogens*, *5*(12), e1000708. https://doi.org/10.1371/journal.ppat.1000708

Giogha, C., Lung, T. W. F., Mühlen, S., Pearson, J. S., & Hartland, E. L. (2015). Substrate recognition by the zinc metalloprotease effector NleC from enteropathogenic Escherichia coli. *Cellular Microbiology*, *17*(12), 1766–1778. https://doi.org/10.1111/cmi.12469

Gomes, T. A. T., Elias, W. P., Scaletsky, I. C. A., Guth, B. E. C., Rodrigues, J. F., Piazza, R. M. F., Ferreira, L. C. S., & Martinez, M. B. (2016). Diarrheagenic Escherichia coli. *Brazilian Journal of Microbiology: [Publication of the Brazilian Society for Microbiology]*, *47 Suppl 1*(Suppl 1), 3–30. https://doi.org/10.1016/j.bjm.2016.10.015

Guignot, J., Segura, A., & Tran Van Nhieu, G. (2015). The Serine Protease EspC from Enteropathogenic Escherichia coli Regulates Pore Formation and Cytotoxicity Mediated by the Type III Secretion System. *PLoS Pathogens*, *11*(7), e1005013. https://doi.org/10.1371/journal.ppat.1005013

Guignot, J., & Tran Van Nhieu, G. (2016). Bacterial Control of Pores Induced by the Type III Secretion System: Mind the Gap. *Frontiers in Immunology*, *7*, 84. https://doi.org/10.3389/fimmu.2016.00084

Hazen, T. H., Donnenberg, M. S., Panchalingam, S., Antonio, M., Hossain, A., Mandomando, I., Ochieng, J. B., Ramamurthy, T., Tamboura, B., Qureshi, S., Quadri, F., Zaidi, A., Kotloff, K. L., Levine, M. M., Barry, E. M., Kaper, J. B., Rasko, D. A., & Nataro, J. P. (2016). Genomic diversity of EPEC associated with clinical presentations of differing severity. *Nature Microbiology*, *1*, 15014. https://doi.org/10.1038/nmicrobiol.2015.14

Jaiswal, J. K., Andrews, N. W., & Simon, S. M. (2002). Membrane proximal lysosomes are the major vesicles responsible for calcium-dependent exocytosis in nonsecretory cells. *The Journal of Cell Biology*, *159*(4), 625–635. https://doi.org/10.1083/jcb.200208154

Li, S., Zhang, L., Yao, Q., Li, L., Dong, N., Rong, J., Gao, W., Ding, X., Sun, L., Chen, X., Chen, S., & Shao, F. (2013). Pathogen blocks host death receptor signalling by arginine GlcNAcylation of death domains. *Nature*, *501*(7466), 242–246. https://doi.org/10.1038/nature12436

Liu, A. R., & Ramakrishnan, P. (2021). Regulation of Nuclear Factor-kappaB Function by O-GlcNAcylation in Inflammation and Cancer. *Frontiers in Cell and Developmental Biology*, *9*, 751761. https://doi.org/10.3389/fcell.2021.751761

Lozer, D. M., Souza, T. B., Monfardini, M. V., Vicentini, F., Kitagawa, S. S., Scaletsky, I. C. A., & Spano, L. C. (2013). Genotypic and phenotypic analysis of diarrheagenic Escherichia coli strains isolated from Brazilian children living in low socioeconomic level communities. *BMC Infectious Diseases*, *13*, 418. https://doi.org/10.1186/1471-2334-13-

Mills, E., Baruch, K., Charpentier, X., Kobi, S., & Rosenshine, I. (2008). Real-time analysis of effector translocation by the type III secretion system of enteropathogenic Escherichia coli. *Cell Host & Microbe*, *3*(2), 104–113. https://doi.org/10.1016/j.chom.2007.11.007

Monjarás Feria, J., García-Gómez, E., Espinosa, N., Minamino, T., Namba, K., & González-Pedrajo, B. (2012). Role of EscP (Orf16) in injectisome biogenesis and regulation of type III protein secretion in enteropathogenic Escherichia coli. *Journal of Bacteriology*, *194*(22), 6029–6045. https://doi.org/10.1128/JB.01215-12

Motolani, A., Martin, M., Wang, B., Jiang, G., Alipourgivi, F., Huang, X., Safa, A., Liu, Y., & Lu, T. (2023). Critical Role of Novel O-GlcNAcylation of S550 and S551 on the p65 Subunit of NF-κB in Pancreatic Cancer. *Cancers*, *15*(19), 4742. https://doi.org/10.3390/cancers15194742

Ornelas-Guevara R, Gil D, Voorsluijs V, Dupont G. Computational investigation of IP_3 diffusion. Sci Rep. 2023 Feb 20;13(1):2922. doi: 10.1038/s41598-023-29876-3. PMID: 36808161; PMCID: PMC9941478.

Özcan, S., Andrali, S. S., & Cantrell, J. E. L. (2010). Modulation of transcription factor function by O-GlcNAc modification. *Biochimica et Biophysica Acta*, *1799*(5–6), 353–364. https://doi.org/10.1016/j.bbagrm.2010.02.005

Pallett, M. A., Berger, C. N., Pearson, J. S., Hartland, E. L., & Frankel, G. (2014). The type III secretion effector NleF of enteropathogenic Escherichia coli activates NF-κB early during infection. *Infection and Immunity*, *82*(11), 4878–4888. https://doi.org/10.1128/IAI.02131-14

Pearson, J. S., Giogha, C., Ong, S. Y., Kennedy, C. L., Kelly, M., Robinson, K. S., Lung, T. W. F., Mansell, A., Riedmaier, P., Oates, C. V. L., Zaid, A., Mühlen, S., Crepin, V. F., Marches, O., Ang, C.-S., Williamson, N. A., O'Reilly, L. A., Bankovacki, A., Nachbur, U., … Hartland, E. L. (2013). A type III effector antagonizes death receptor signalling during bacterial gut infection. *Nature*, *501*(7466), 247–251. https://doi.org/10.1038/nature12524

Pearson, J. S., Giogha, C., Lung, T. W. F., & Hartland, E. L. (2016). The Genetics of Enteropathogenic Escherichia coli Virulence. *Annual Review of Genetics*, *50*(Volume 50, 2016), 493–513. https://doi.org/10.1146/annurev-genet-120215-035138

Ramachandran, R. P., Spiegel, C., Keren, Y., Danieli, T., Melamed-Book, N., Pal, R. R., Zlotkin-Rivkin, E., Rosenshine, I., & Aroeti, B. (2020). Mitochondrial Targeting of the Enteropathogenic Escherichia coli Map Triggers Calcium Mobilization, ADAM10-MAP Kinase Signaling, and Host Cell Apoptosis. *mBio*, *11*(5), e01397-20. https://doi.org/10.1128/mBio.01397-20

Ruan, H.-B., Ma, Y., Torres, S., Zhang, B., Feriod, C., Heck, R. M., Qian, K., Fu, M., Li, X., Nathanson, M. H., Bennett, A. M., Nie, Y., Ehrlich, B. E., & Yang, X. (2017). Calcium-dependent O-GlcNAc signaling drives liver autophagy in adaptation to starvation. *Genes & Development*, *31*(16), 1655–1665. https://doi.org/10.1101/gad.305441.117

Ruchaud-Sparagano, M.-H., Mühlen, S., Dean, P., & Kenny, B. (2011). The enteropathogenic E. coli (EPEC) Tir effector inhibits NF-κB activity by targeting TNF-α receptor-associated factors. *PLoS Pathogens*, *7*(12), e1002414. https://doi.org/10.1371/journal.ppat.1002414

Sal-Man, N., Deng, W., & Finlay, B. B. (2012). EscI: A crucial component of the type III secretion system forms the inner rod structure in enteropathogenic Escherichia coli. *The Biochemical Journal*, *442*(1), 119–125. https://doi.org/10.1042/BJ20111620

Savio LEB, de Andrade Mello P, da Silva CG, Coutinho-Silva R. The P2X7 Receptor in Inflammatory Diseases: Angel or Demon? Front Pharmacol. 2018 Feb 6;9:52. doi: 10.3389/fphar.2018.00052. PMID: 29467654; PMCID: PMC5808178.

Serapio-Palacios, A., & Navarro-Garcia, F. (2016). EspC, an Autotransporter Protein Secreted by Enteropathogenic Escherichia coli, Causes Apoptosis and Necrosis through Caspase and Calpain Activation, Including Direct Procaspase-3 Cleavage. *mBio*, *7*(3), e00479-16. https://doi.org/10.1128/mBio.00479-16

Shtuhin-Rahav, R., Olender, A., Zlotkin-Rivkin, E., Bouman, E. A., Danieli, T., Nir-Keren, Y., Weiss, A. M., Nandi, I., & Aroeti, B. (2023). Enteropathogenic E. coli infection co-elicits lysosomal exocytosis and lytic host cell death. *mBio*, *14*(6), e01979-23. https://doi.org/10.1128/mbio.01979-23

Smedler E, Uhlén P. Frequency decoding of calcium oscillations. Biochim Biophys Acta. 2014 Mar;1840(3):964-9. doi: 10.1016/j.bbagen.2013.11.015. Epub 2013 Nov 22. PMID: 24269537.

Swillens S, Dupont G, Combettes L, Champeil P. From calcium blips to calcium puffs: theoretical analysis of the requirements for interchannel communication. Proc Natl Acad Sci U S A. 1999 Nov 23;96(24):13750-5. doi: 10.1073/pnas.96.24.13750. PMID: 10570144; PMCID: PMC24136.

Szabadkai, G., Simoni, A. M., & Rizzuto, R. (2003). Mitochondrial Ca2+ uptake requires sustainedCa2+ release from the endoplasmic reticulum. *The Journal of Biological Chemistry*, *278*(17), 15153–15161. https://doi.org/10.1074/jbc.M300180200

Tsunemi, T., Perez-Rosello, T., Ishiguro, Y., Yoroisaka, A., Jeon, S., Hamada, K., Rammonhan, M., Wong, Y. C., Xie, Z., Akamatsu, W., Mazzulli, J. R., Surmeier, D. J., Hattori, N., & Krainc, D. (2019). Increased Lysosomal Exocytosis Induced by Lysosomal Ca2+ Channel Agonists Protects Human Dopaminergic Neurons from α-Synuclein Toxicity. *Journal of Neuroscience*, *39*(29), 5760–5772. https://doi.org/10.1523/JNEUROSCI.3085-18.2019

Vandeput, F., Combettes, L., Mills, S. J., Backers, K., Wohlkönig, A., Parys, J. B., De Smedt, H., Missiaen, L., Dupont, G., Potter, B. V. L., & Erneux, C. (2007). Biphenyl 2,3',4,5',6-pentakisphosphate, a novel inositol polyphosphate surrogate, modulates Ca2+ responses in rat hepatocytes. *FASEB Journal: Official Publication of the Federation of American Societies for Experimental Biology*, *21*(7), 1481–1491. https://doi.org/10.1096/fj.06-7691com

Voorsluijs V, Dawson SP, De Decker Y, Dupont G. Deterministic Limit of Intracellular Calcium Spikes. Phys Rev Lett. 2019 Mar 1;122(8):088101. doi: 10.1103/PhysRevLett.122.088101. PMID: 30932600.

Yan, D., Quan, H., Wang, L., Liu, F., Liu, H., Chen, J., Cao, X., & Ge, B. (2013). Enteropathogenic *Escherichia coli* Tir recruits cellular SHP-2 through ITIM motifs to suppress host immune response. *Cellular Signalling*, *25*(9), 1887–1894. https://doi.org/10.1016/j.cellsig.2013.05.020

Yen, H., Ooka, T., Iguchi, A., Hayashi, T., Sugimoto, N., & Tobe, T. (2010). NleC, a Type III Secretion Protease, Compromises NF-κB Activation by Targeting p65/RelA. *PLOS Pathogens*, *6*(12), e1001231. https://doi.org/10.1371/journal.ppat.1001231

Zhang, L., Ding, X., Cui, J., Xu, H., Chen, J., Gong, Y.-N., Hu, L., Zhou, Y., Ge, J., Lu, Q., Liu, L., Chen, S., & Shao, F. (2011). Cysteine methylation disrupts ubiquitin-chain sensing in NF-κB activation. *Nature*, *481*(7380), 204–208. https://doi.org/10.1038/nature10690

Zhong, Q., Roumeliotis, T. I., Kozik, Z., Cepeda-Molero, M., Fernández, L. Á., Shenoy, A. R., Bakal, C., Frankel, G., & Choudhary, J. S. (2020). Clustering of Tir during enteropathogenic E. coli infection triggers calcium influx–dependent pyroptosis in intestinal epithelial cells. *PLoS Biology*, *18*(12), e3000986. https://doi.org/10.1371/journal.pbio.3000986

Zhong, Q., Chatterjee, S., Choudhary, J. S., & Frankel, G. (2022). EPEC-induced activation of the Ca2+ transporter TRPV2 leads to pyroptotic cell death. *Molecular Microbiology*, *117*(2), 480–492. https://doi.org/10.1111/mmi.14863

Figures and Legends

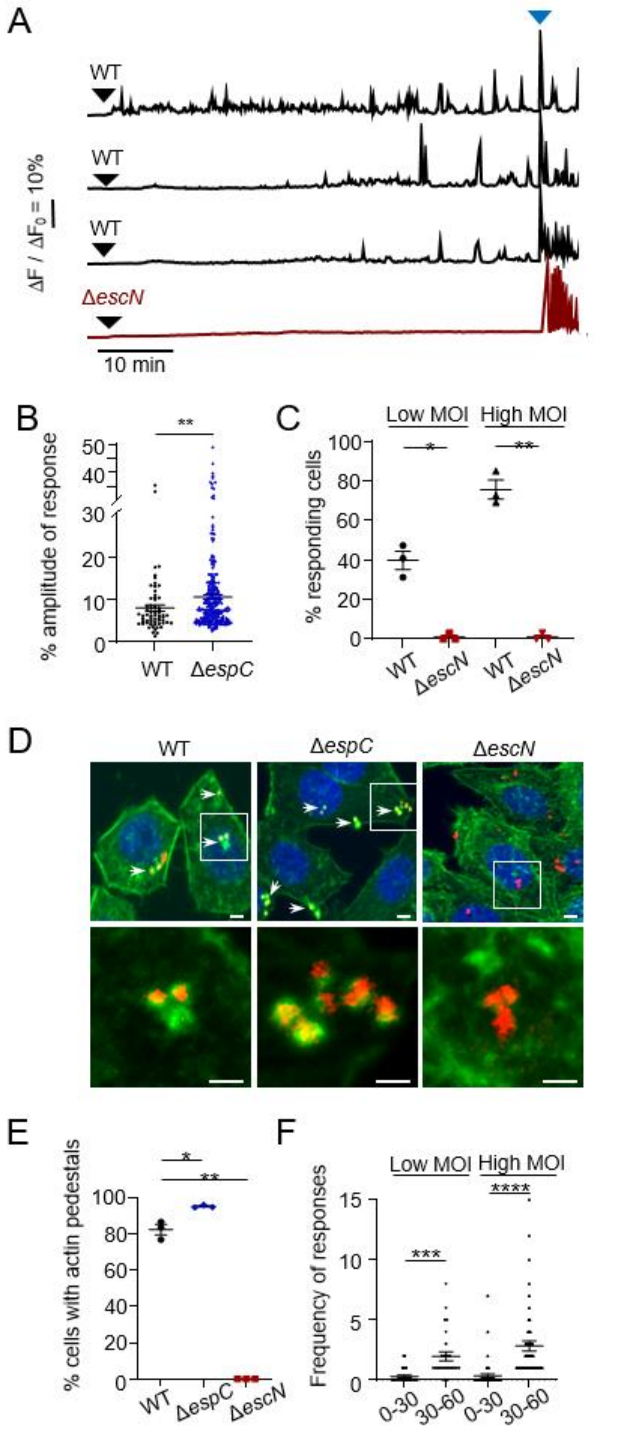

Figure 1. EPEC induces isolated Ca^{2+} responses of limited amplitude in epithelial cells.

HeLa cells were loaded with the fluorescent indicator Cal-520, challenged with the indicated bacteria and subjected to live-cell Ca^{2+} imaging at a frequency of one acquisition every 10 seconds (**A-C, F**) or fixed and processed for fluorescence microscopy analysis (**D-E**) (Materials and Methods). **A**,

Representative traces of Ca^{2+} variations in single cells. The black arrowheads indicate the time of bacterial challenge. The blue arrowheads indicate stimulation with 3 µM histamine. **B**, Response amplitude expressed as a percent of the maximal histamine response amplitude (N = 3, n > 63). **C**, Percent of cells exhibiting Ca^{2+} responses (N =3, n > 66). (**D, E**) Cells challenged with RFP-expressing bacteria for 1 hour. **D**, Representative confocal micrographs. Staining with DAPI (blue), phalloidin-Alexa 488 (green). The lower panels show a higher magnification of the insets in the top panels. Scale bar = 10 µm. **E**, Percentage of bacteria-associated actin-rich pedestals (N = 3, n > 273). **F**, average number of responses per cell during the first 30 min (0-30) and last 30 min (30-60) of bacterial challenge. Low MOI: 10 bacteria / cell. High MOI: 50 bacteria / cell. Bar: mean. (N = 3, n > 63). Mann-Whitney test. *: $p < 0.05$; **: $p < 0.01$; ***: $p < 0.001$; ****: $p < 0.0001$.

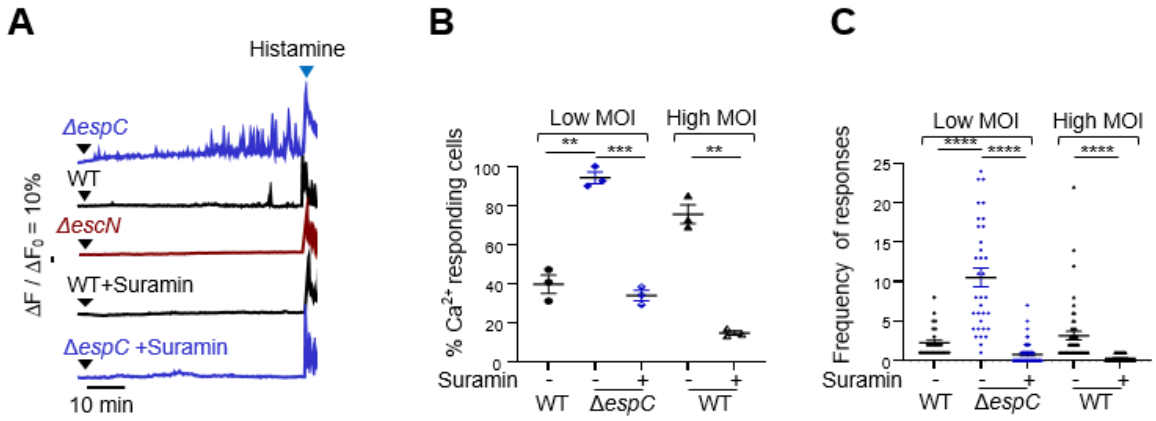

Figure 2. EPEC-induced Ca^{2+} responses are elicited by ATP released by the T3SS translocon

HeLa cells were loaded with the fluorescent indicator Cal-520 or with 200 µM suramin for 30 minutes, challenged with the indicated bacteria and subjected to live-cell Ca^{2+} imaging for a 60 min-duration at a frequency of one acquisition every 10 seconds. **A**, Representative traces of Ca^{2+} variations in single cells. The black arrowheads indicate the time of bacterial challenge. The blue arrowheads indicate stimulation with 3 µM histamine. **B**, Percent of cells exhibiting Ca^{2+} responses (N = 3, n > 66). **C**, Average number of responses per cell. Low MOI: 10 bacteria / cell. High MOI: 50 bacteria / cell. Bar: mean. (N = 3, n > 30). Mann-Whitney test. **: $p < 0.01$; ***: $p < 0.001$; ****: $p < 0.0001$.

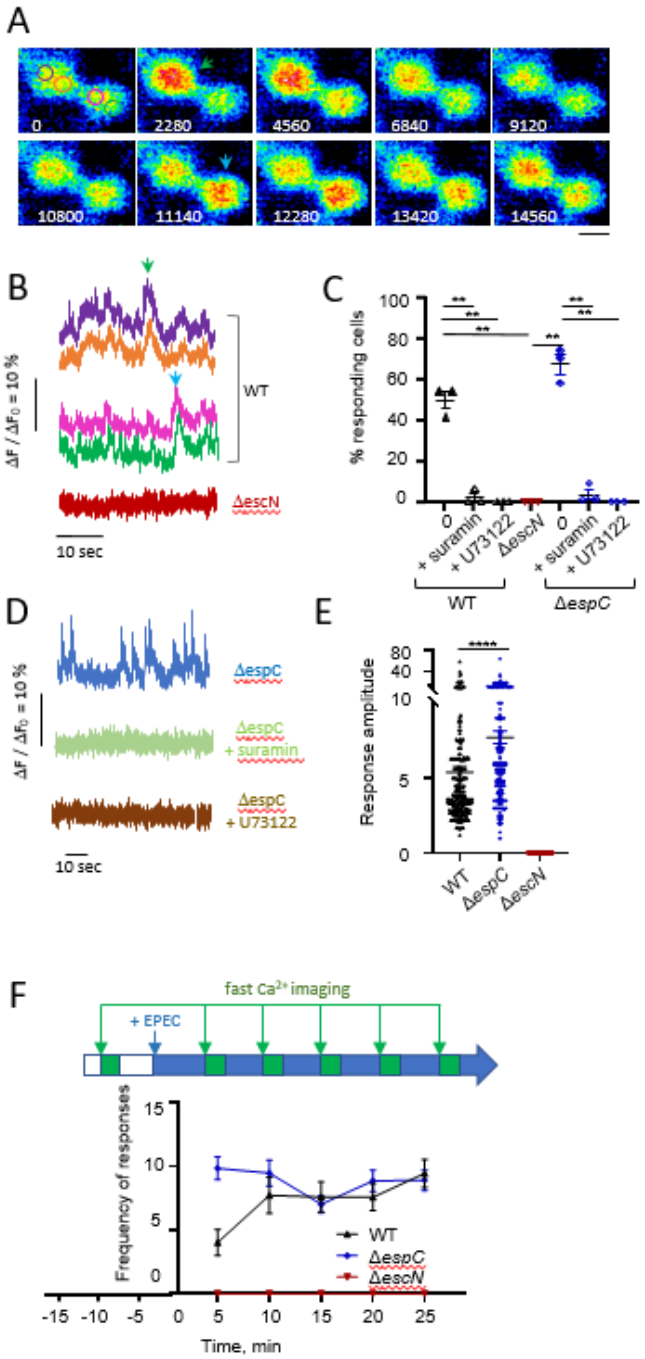

Figure 3. EPEC induces rapid and Coordinated Elementary Ca^{2+} Responses.

HeLa cells were loaded with the fluorescent indicator Cal-520, challenged with the indicated bacteria and subjected to high speed Ca^{2+} imaging at a frequency of one acquisition every 57 ms for a duration of 110 seconds. **A**, Representative time-serie of pseudocolored fluorescent micrographs of cells challenged with wild-type EPEC. The numbers indicate the elapsed time in ms from an arbitrarily determined origin. Scale bar = 10 µm. **B**, **D**, traces of Ca^{2+} variations in 2 subcellular regions of the same cell. **B**, WT: traces corresponding to the regions depicted in the image 0 of panel **A**. The arrowheads

point to the Ca^{2+} responses shown in Panel A with the corresponding color. **C**, Percent of cells exhibiting Ca^{2+} responses (N > 3, n > 256). + Suramin: treatment with 200 µM Suramin. +U73122: treatment with 10 µM U73122. **E**, Response amplitude expressed as a percent of the maximal response amplitude induced by treatment with 3 µM histamine (N = 3, n > 20). **F**, average number of responses per cell. **C**, **E**, Bar: mean. Mann-Whitney test. **: $p < 0.01$; ****: $p < 0.0001$. **F**, High speed Ca^{2+} imaging was performed every 5 min for 110 seconds following infection with the indicated bacterial strain as depicted the scheme. The average number of responses per cell is indicated (N > 3, n > 29).

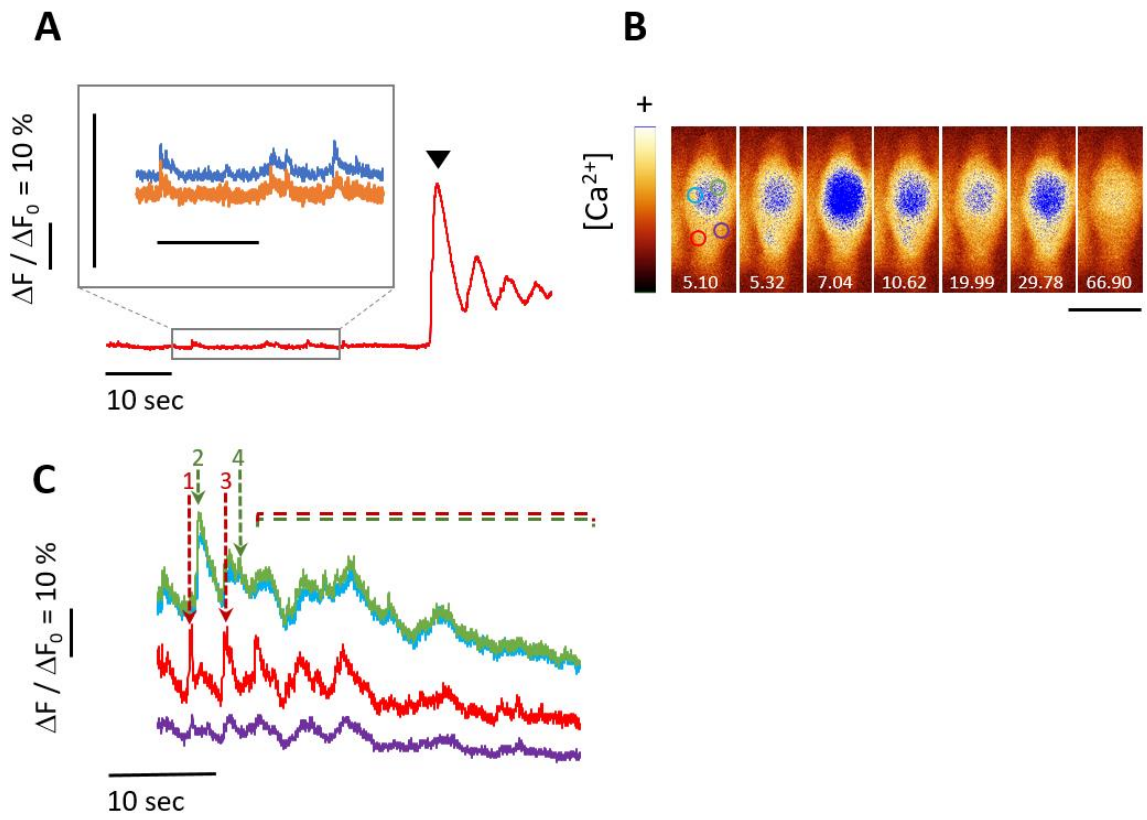

Fig. 4: EPEC-induced Coordinated Elementary Ca^{2+} Responses are reproduced by low ATP levels.

A-**C**, HeLa cells were loaded with the fluorescent indicator Cal-520, challenged with 150 nM ATP and subjected to Ca^{2+} imaging. Image acquisition every 2 s (**A**) or 22 ms (**B**, **C**). **A**, Traces of Ca^{2+} variations corresponding to a single cell (red trace), or subcellular regions within the same cell (inset). **A**, arrowhead: challenge with 2 µM ATP. **B**, Time serie of fluorescent micrographs pseudocolored using the "glow" Fiji lookup table, where the blue pixel correspond to an arbitrarily set threshold value. The numbers indicate the elapsed time in seconds. Blue: high intensity pixels showing the large top cell area with CCRICs and the local lower puff area. Scale bar = 10 µm. **C**, Traces corresponding to Ca^{2+} variations in the subcellular regions depicted in Panel **B**. The responses are labelled 1-4, with the response 1 corresponding to the puff (Panel **B**, red ROI) impulsing the response 3 in the same region. Responses 2 and 4 correspond to CCRICs in Panel **B**, blue and green ROIs. Note the diffusion of the responses from the initial release area in other area inferred from the dampening of the response amplitude. The dashed red and green lines point at the aggregation of responses throughout the cell.

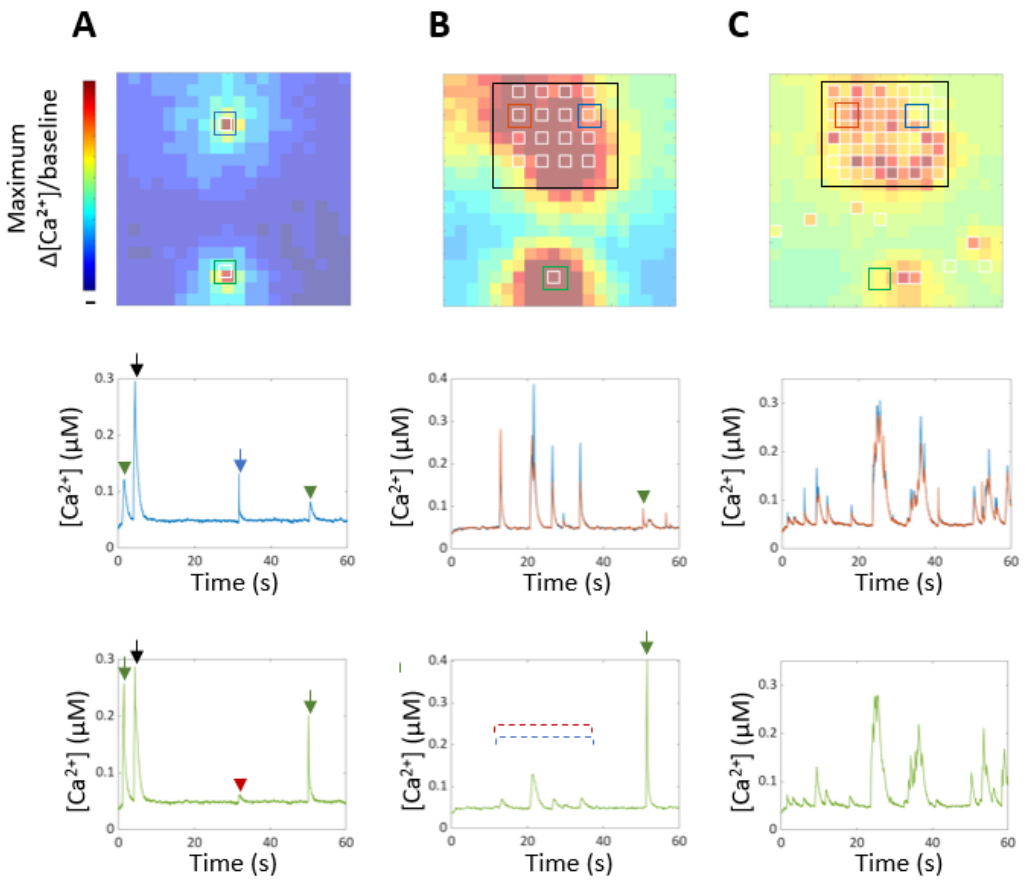

Fig. 5. Modeling of Coordinated Elementary Ca^{2+} Responses.

Top, Ca^{2+} variations in subcellular area within a single cell are represented in pseudocolor. Shown are the maximum values of $\Delta[Ca^{2+}]/[Ca^{2+}]_b$ reached in each compartment during a 60s simulation. Empty white squares: IP_3R clusters. **Graphs**, Traces correspond to Ca^{2+} variations in the region with the matching color. Colored arrows: Ca^{2+} response due to the activation of an IP_3 cluster in the region with the matching color. Colored arrowhead and dashed red and blue lanes: Ca^{2+} variations due to the diffusion of a Ca^{2+} response from or nearby to the region with the matching color. Black arrows: Ca^{2+} response due Ca^{2+}-activated Ca^{2+} release. **A**, low density of IP_3R clusters with local responses detected. **B**, **C**, Empty black box: area with a high density IP_3R clusters. **C**, similar to **B**, but following IP_3R cluster sensitization due to increased Ca^{2+} responses.

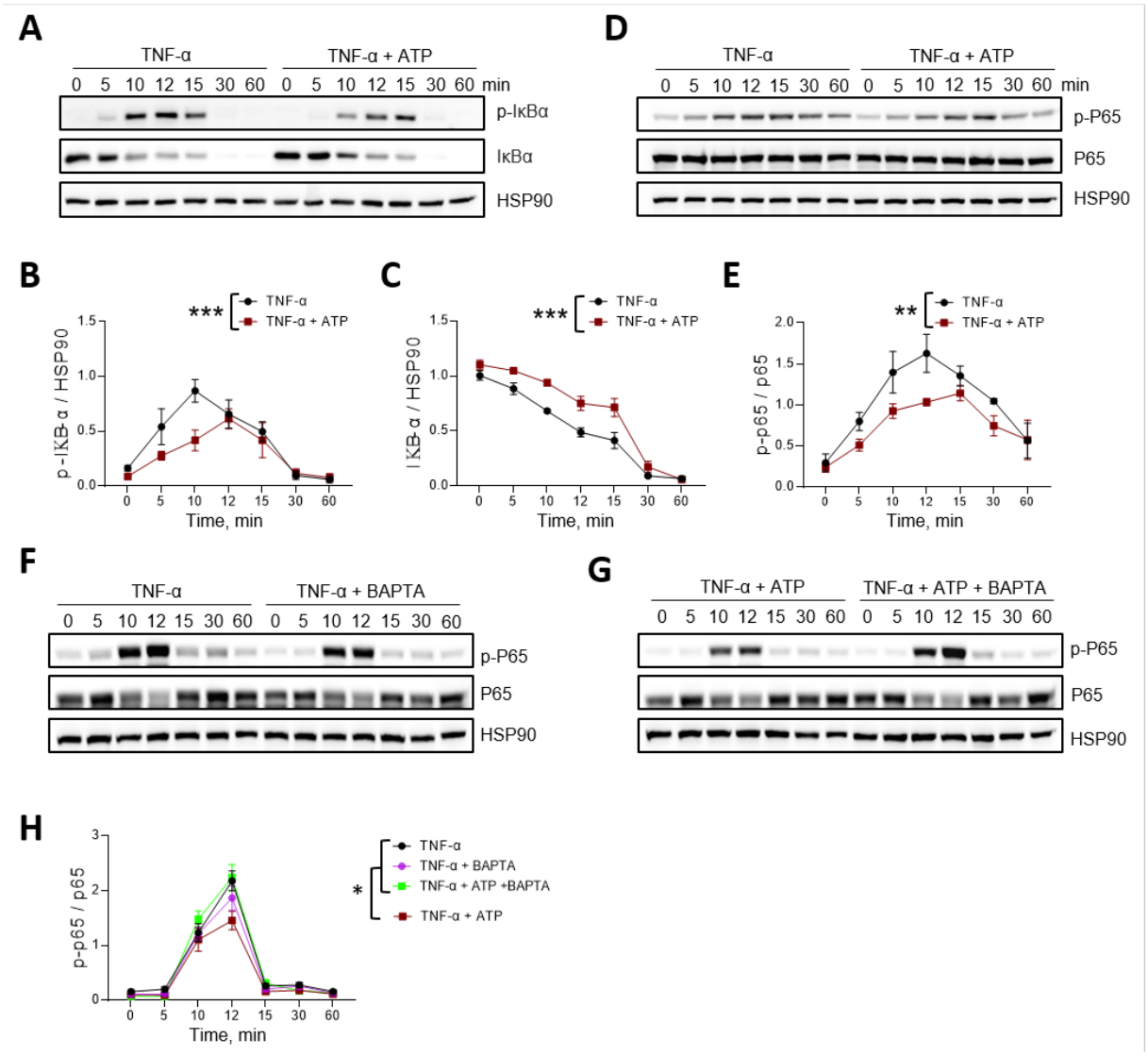

Fig. 6. Low ATP levels dampen NF-kappaB activation.

HeLa cells were stimulated with 10 ng/ml TNF-α alone or in the presence of 150 nM ATP or 20 μM BAPTA-AM (**F**-**H**). At the indicated time points, cell lysates were analyzed by Western blot using the indicated antibodies**. A**, **D**, **F**, **G**, Representative blots. **B**-**E**, **H**, Densitometry analysis of the indicated antibody signal normalized to that of HSP90 (**B, C, F**) or total P65 (**E**). p-P65: anti-phospho P65 antibody. P-IκB: anti-phospho IκB antibody. ANCOVA test. *: $p < 0.05$; **: $p < 0.01$; ***: $p < 0.001$.

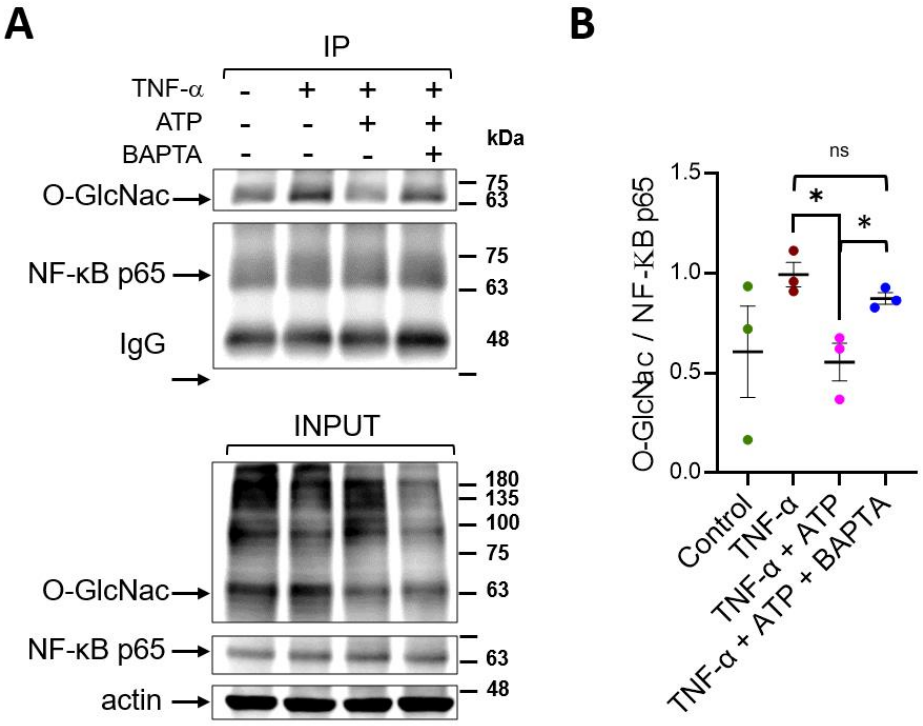

Fig. 7. Low ATP levels down-regulate NF-kB O-GlcNAcylation in a Ca^{2+}-dependent manner. HeLa cells were stimulated with 10 ng/ml TNF-α alone or in the presence of 150 nM ATP or 20 μM BAPTA-AM for 12 min. Cell lysates were subjected to P65 immunoprecipitation. **A**, Representative blots with the indicated antibodies. IP: immunoprecipitates ; L: total cell lysates. **B**, Densitometry analysis of the O-GlucNAc signal in P65 immunoprecipitates normalized to that of TNF-α alone. Mann-Whitney test. N = 4. *: $p < 0.05$. ns: not significant.

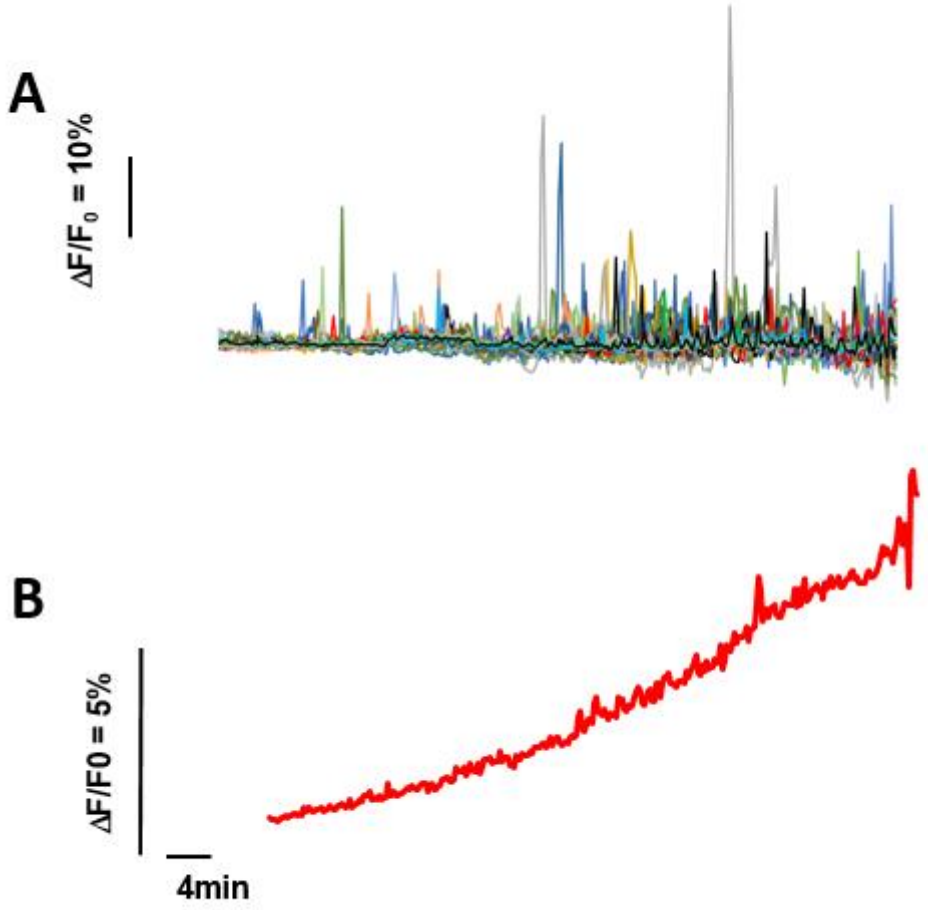

Fig. S1. EPEC induces Ca^{2+} responses with a frequency increasing during the time of infection.

Ca^{2+} imaging was performed on HeLa cells loaded with the Ca^{2+} fluorescent indicator Cal-520 and challenged with EPEC at a MOI of 100. A, Traces of Ca^{2+} variations in single cells. B, Trace corresponding to the average of traces shown in B (n=32). Note that cells do not show an increase in basal Ca^{2+} levels that could be mistakenly interpreted from the averaging of Ca^{2+} responses over the cell population.

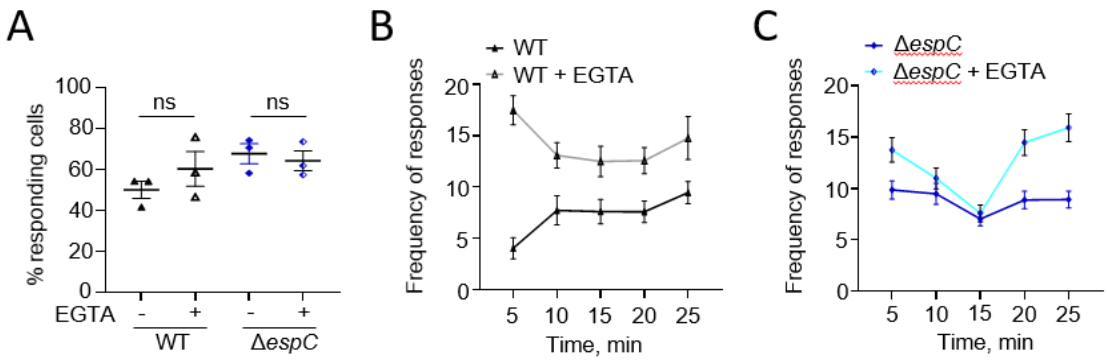

Fig. S2. EGTA does not inhibit EPEC-induced Ca^{2+} responses.

HeLa cells were challenged with a high MOI of EPEC wild-type (WT) or a low MOI of the *ΔespC* mutant. + EGTA: cells treated with 4 mM EGTA. **A**, Percent of cells showing Ca^{2+} responses. **B**, **C**, Frequency of Ca^{2+} responses per cell.

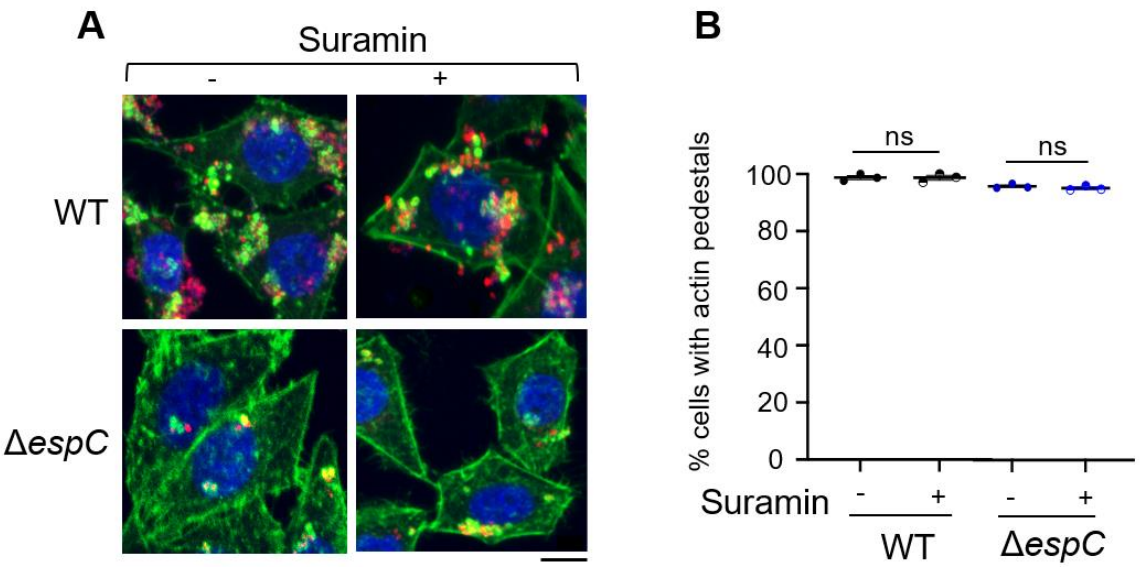

Figure S3. Suramin does not affect EPEC-Induced actin pedestals

HeLa cells were challenged with the indicated RFP-expressing bacterial strains in the presence or absence of 200 μM suramin. Samples were fixed and processed for fluorescence staining. **A**, Representative micrographs. Blue: DAPI; green: Phalloidin-Alexa488; red: bacteria. Scale bar = 10 μm. **B**, Percent of cells exhibiting actin-rich pedestals. High MOI: 50 bacteria / cell. Low MOI *ΔespC*: 10 bacteria / cell. (N=3, n > 273). Mann Whitney test. ns: not significant.

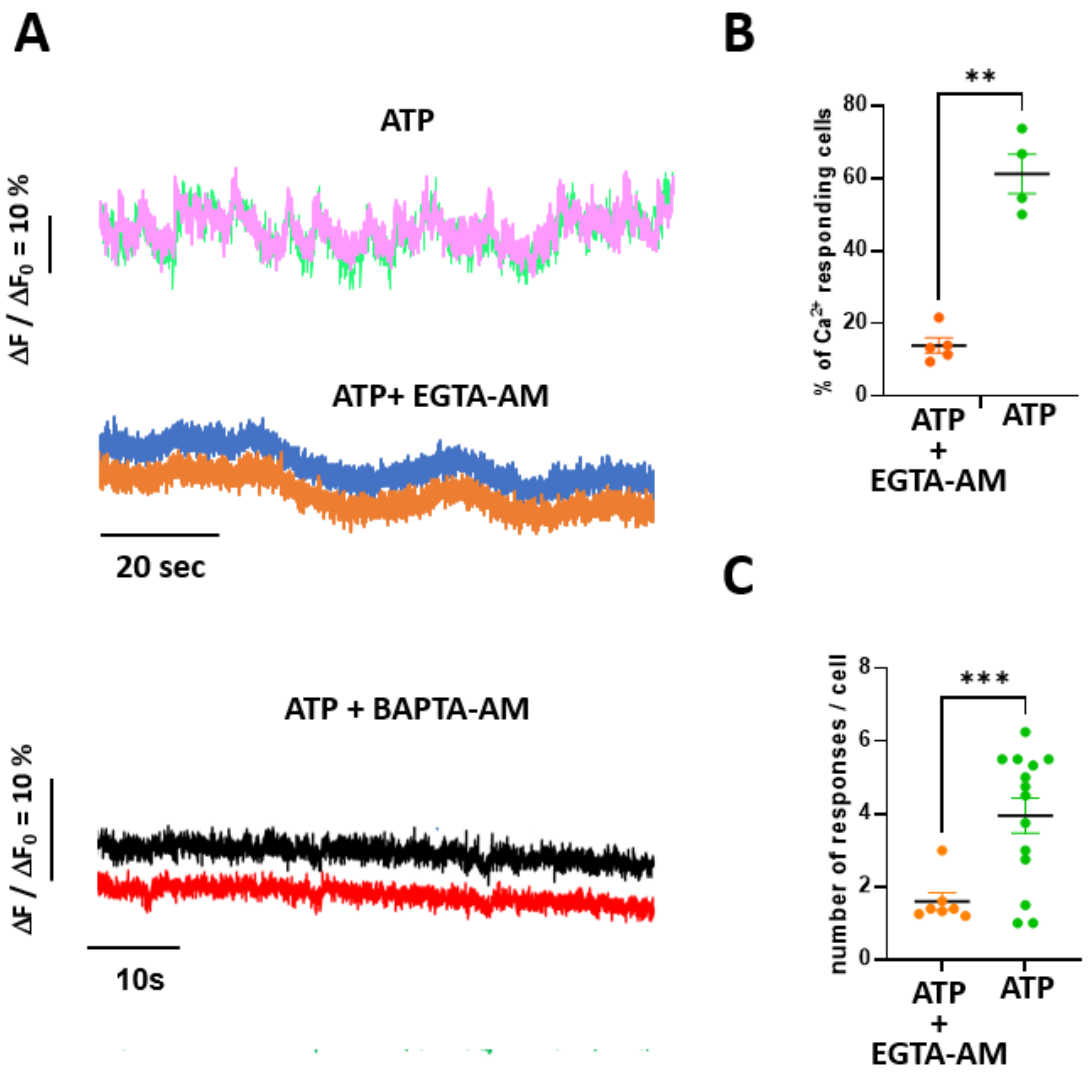

Fig. S4. Intracellular Ca^{2+} chelation inhibits CCRICs.

HeLa cells were loaded with the fluorescent indicator Cal-520 in the presence or absence of 20 µM EGTA-AM or BAPTA-AM. Samples were stimulated with 150 nM ATP and subjected to high speed Ca^{2+} imaging at a frequency of one acquisition every 22 ms. **A**, Representative traces of Ca^{2+} variations in 2 subcellular regions of the same cell. No Ca^{2+} responses were observed for cells treated with BAPTA-AM (N = 3, > 65 cells). **B**, Percent of cells exhibiting Ca^{2+} responses (N > 3, n > 62). **C,** average number of responses per cell. (N > 3, n > 62). Mann-Whitney test. **: $p < 0.01$; ***: $p < 0.001$.

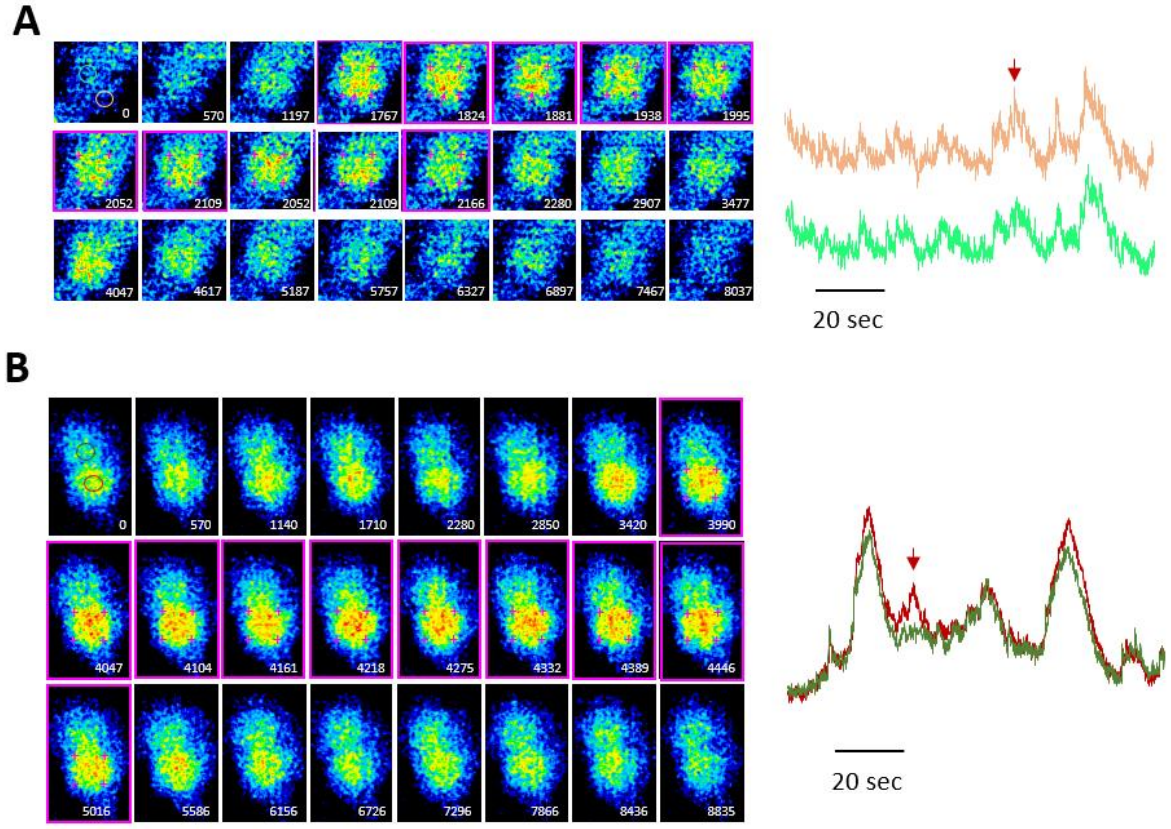

Fig. S5. CCRICs induced by EPEC result from Ca^{2+} released by highly transient or mobile IP_3R clusters. Time series of HeLa cells loaded with Cal-520 and challenged with wild type EPEC at a MOI of 50 bacteria / cell. Time is indicated in ms. Traces: variations of Ca^{2+} in ROI depicted at T = 0 in the corresponding color. The red arrow points at the response peak illustrated by the time series. Images framed in purple are taken at 57 ms interval. The marks inside the frame aim at better highlighting cluster / channel mobility. Cal-520 intensity in pseudocolor. **A**, Globally Coordinated responses associated with small and highly mobile clusters. Note the bigger and less mobile cluster (purple arrow). **B**, Puff-like response.

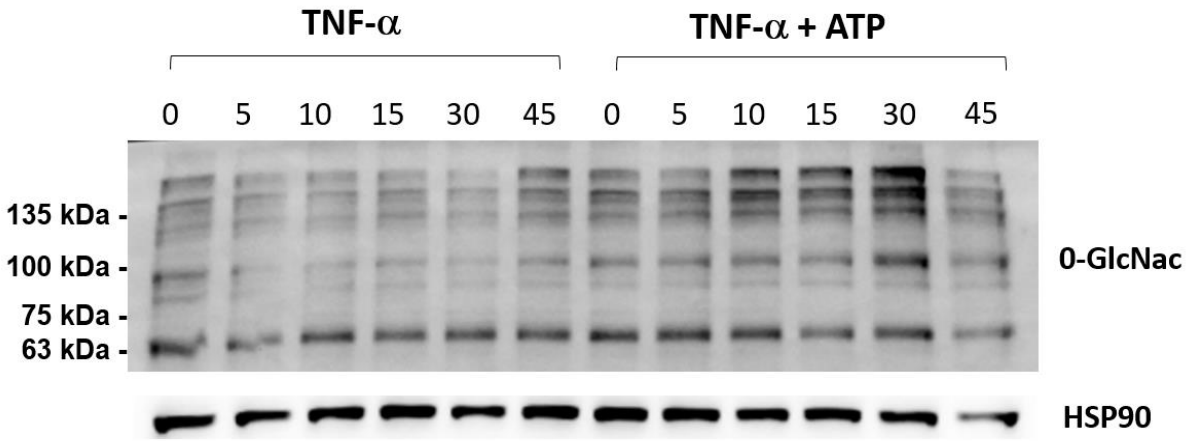

Fig. S6. Effects of ATP on TNF-α-induced profiles of O-GlcNacylation in HeLa cells. HeLa cells were stimulated with 10 ng/ml TNF-α alone or co-stimulated with 10 ng/ml TNF-α and 150 nM ATP. Representative blots of cell lysates analyzed by Western blot at the time points indicated in minutes using the indicated antibodies.

Supplementary Methods.

Following previous modeling studies of Ca^{2+} dynamics (Voorsluijs et al., 2019; Ornelas-Guevara et al. 2023), we implement a fully stochastic model of intracellular Ca^{2+} dynamics using the Gillespie algorithm. The model captures IP_3-induced Ca^{2+} release from IP_3R clusters, SERCA-mediated reuptake, ER Ca^{2+} leak, and cytosolic Ca^{2+} diffusion. The simulated HeLa cell is represented as a 10 × 10 μm^2 square, discretized into a 20 × 20 grid. Each compartment (0.5 × 0.5 μm^2) corresponds to a cytosolic volume of 10^{-16} L.

Each IP_3R cluster is represented as a single unit with four discrete states: Open (**O**), Closed (**C**), and two inhibited states (**i_1**, **i_2**). The transition from **C** to **O** depend on both [Ca^{2+}] and [IP_3], while the transition from **O** to **i1** depends on [Ca^{2+}], following the model described in Ornelas-Guevara et al., 2023 (see Figure S1). Various spatial distributions of the IP_3R clusters are investigated in Figure 5A to 5C, where the locations of the clusters are indicated by white boxes. SERCA activity and ER Ca^{2+} leak are present in all compartments.